Polymer Bulletin (2020) 77:4381–4400
https://doi.org/10.1007/s00289-019-02973-y

ORIGINAL PAPER

Eco-friendly conductive polymer-based nanocomposites, $BiVO_4$/graphene oxide/polyaniline for excellent photocatalytic performance

Md. Rokon Ud Dowla Biswas[1] · Bang Seong Ho[2] · Won-Chun Oh[1]

Received: 21 June 2019 / Revised: 21 September 2019 / Accepted: 24 September 2019 /
Published online: 27 September 2019
© Springer-Verlag GmbH Germany, part of Springer Nature 2019

Abstract

In this study, we describe the structure of bismuth vanadate ($BiVO_4$)/graphene oxide/polyaniline (PANI) compound with exploited interfacial coupling, their use as visible-light photocatalysts and safety property. Thin graphene oxide sheets could completely cover $BiVO_4$ polyhedrons with vastly conductive polymer PANI through an evaporation-induced hydrothermal process. The enhanced surface adsorption outcome of GO, a huge improvement in the photoactivity of $BiVO_4$, has been proved through the degradation of methylene blue (MB) and safranin O (SO) upon the covering of polyaniline. The improved photocatalytic activity is recognized for the development of well-defined $BiVO_4$/GO/PANI interfaces which considerably increases the charge separation efficacy. Conversely, safety aspects are investigated for identifying the toxicity of samples on the different kinds of bacteria. Our study found that in the existence of every sample the bacteria could not be killed throughout the culture medium. Considering its ease of preparation and excellent performance, $BiVO_4$/GO/PANI could be a promising, competitive and safe visible-light-driven photocatalyst in the field of environmental remediation.

Keywords Safety aspects · Bacteria · Nanocomposite · Environmental safety

Introduction

Since the start of the twenty-first century, water pollution has been a big problem which exerts serious effects on the ecological atmosphere and human survival [1, 2]. Organic dyes [3, 4], benzene-based organics [5, 6] and phenol [7, 8] are the key

✉ Won-Chun Oh
wc_oh@hanseo.ac.kr

[1] Department of Advanced Materials Science and Engineering, Hanseo University, Seosan-si, Chungnam 356-706, Korea

[2] Department of Biological Sciences, Hanseo University, 46 Hanseo 1-ro, Haemi-myen, Seosan-si, Choongnam-do 356-706, Korea

pollutants of concern in wastewater owing to their high toxicity and almost non-degradable characteristics. Therefore, seeking efficient, green and non-toxic purification technology and material that can efficiently eliminate organic toxins from wastewater is of great importance for environmental safety. Compared with the conventional methods, photocatalysis technology shows greater promise in environmental remediation because of its low cost, lack of harmful by-products and durable oxidative capability for contaminants under facile conditions [9–12].

In contrast, materials with delocalized conjugated forms have been broadly studied, owing to their quick photoinduced charge separation and relatively slow-moving charge recombination [13]. Polyaniline (PANI), a conducting polymer with an unmitigated π-conjugated electron system, has recently shown immense assure because of its good absorption coefficients in the visible-light range and extraordinary mobility of charge carriers [14].

Furthermore, PANI, in its undoped or partially doped states, acts as an electron contributor upon photoexcitation and is recognized as a respectable hole conductor which can carry a current of several milliamperes [15]. Moreover, compared to doped materials such as noble metal, PANI is more in practice for its relative ease of commercial-scale production. Considering the well-organized carrier transfer character of PANI, it is projected that the mixture of photocatalyst and PANI seems ideal for enhancing the photoactivity under visible light. There are only a few studies published on the amalgamation of PANI and simple metal oxide catalysts to grow their photocatalytic performance [12, 16–19]. Therefore, further research is desired to extend its uses. Bismuth vanadate ($BiVO_4$) has been recognized as a photocatalyst for water splitting [20–22] and the destruction of dye pollutants with extraordinary mineralization [23–29] under visible-light irradiation. Moreover, the discoloration of the dye and photocatalytic degradation of phenol on $BiVO_4$ was also reported [30, 31]. Phenol is widely recognized as a carbon-based chemical that is present in a variety of wastewaters from different industries and is relatively poisonous and sluggish to decompose in the environment [32]. The need to find a good photocatalyst for phenol removal is a trouble of extraordinary environmental concern [33]. The action of pure $BiVO_4$ is stumpy, because of its reduced adsorptive performance and complex movement of electron–hole pairs [34]. Graphene, a two-dimensional (2D) single atomic sheet of sp^2-hybridized carbon atoms, has attracted great interest over the past decade owing to its unexpected electrical properties, optical transparency and biocompatibility [35, 36]. Graphene oxide (GO) is a water-dispersible graphene sheet with carboxylic, phenol hydroxyl and epoxide groups on its edges and basal planes, which can be produced by the chemical oxidation of graphite and consequent exfoliation [37, 38]. Based on its aqueous stability, low production cost and amphiphilic behavior [39–41], GO is a favorable material as a building block for graphene-based nanomaterials and their different uses such as conductive thin film, biosensors and biomedical devices [42, 43]. Additionally, it is value noticing that there has been no report on the synthesis and photoactivity in the $BiVO_4$/GO/PANI system. It is important to twitch complete lessons on the pathway and mechanism of photoinduced electron–hole pairs under visible-light irradiation, to project more efficient visible-light-focused photocatalytic combined materials that will come across the prerequisite of the applied environmental application. Herein, for the first time,

spherical-like $BiVO_4$/GO/PANI photocatalyst was prepared by the hydrothermal method. The work is mostly focused on the visible-light-induced photodegradation of the broadly used organic pollutants, methylene blue (MB) and safranin O. The existence of free electron was also observed, by the measurement of the electrical properties, further demonstrating the photocatalytic performance of $BiVO_4$/GO/PANI. The photodegraded mechanism of $BiVO_4$/GO/PANI photocatalyst was discussed, and the improved photoactivity came from the upgrade of charge separation efficacy caused by the synergy among PANI and $BiVO_4$/GO.

Experimental section

PANI (molecular weight ~ 10^5) was purchased from Jilin Zhengji Corp. All the other reagents used in our experiments were of investigative purity and were used as received from Dejone Chemical Co., Korea.

Bismuth vanadate ($BiVO_4$) synthesis

In a typical synthesis of bismuth vanadate, 0.1896 g of $Bi(NO_3)_3{\cdot}5H_2O$ and 0.0630 g of NH_4VO_3 were individually added to two solutions of absolute ethanol (10 mL), while stirring for over 30 min at room temperature. The above two systems were then combined, adjusted to a pH of 8.0 with an ammonia solution and stirred for 40 min to yield a stable yellow-colored slurry. The resultant combination was then transferred to a 40-mL Teflon-lined stainless steel autoclave and heated to 180 °C for 8 h under autogenous pressure. The reaction mixture is then allowed to cool to room temperature, and the precipitate was sieved, washed with DI water five times and then dehydrated in a vacuum oven at 60 °C for 12 h. A yellowish-colored powder-type sample was finally obtained and labeled as $BiVO_4$.

Synthesis of $BiVO_4$–graphene oxide composite photocatalyst

The representative preparation of $BiVO_4$/GO was as follows: Graphene oxide (GO) was manufactured rendering to the method described by Hummers and Offeman [43] from cleaned natural graphite with a mean particle size of 40 nm, which was bought from the Qingdao Zhongtian Company. $BiVO_4$/GO was fashioned by the use of the facile hydrothermal method.

A characteristic experiment for the synthesis of $BiVO_4$–graphene composite is as follows. First, 50 mg of GO (4% mass ratio) was dispersed into 20 mL of absolute ethanol and 15 mL of deionized (DI) water, with sonication for 2 h. Then, 0.1896 g of $Bi(NO_3)_3{\cdot}5H_2O$ and 0.0630 g of NH_4VO_3 were individually added to two solutions of absolute ethanol (10 mL), while stirring for over 30 min at room temperature. The above three systems were then combined, adjusted to a pH of 8.0 with an ammonia solution and stirred for 40 min, to yield a stable bottle-green-colored slurry. The resultant combination was then moved to a 40-mL Teflon-lined stainless steel autoclave and heated to 180 °C for 8 h under autogenous pressure. The

reaction mixture was then allowed to cool to room temperature, and the precipitate was sieved, washed with DI water five times and then dehydrated in a vacuum oven at 60 °C for 12 h. A greenish-colored powder-type sample was finally obtained and labeled as $BiVO_4$/GO.

Preparation of composite catalysts

The classic preparation of $BiVO_4$/GO/PANI photocatalyst is as follows: PANI was liquefied in tetrahydrofuran (THF) to acquire a concentration of 0.081 g L^{-1} solutions; then, a certain amount of $BiVO_4$/GO powder was added to 100 mL of the above solution. The suspension was then ultrasonicated for a minimum of 2 h, stirred for 4 h and then filtered. The as-produced precipitate was then washed with water thrice and then dried at 70 °C for 13 h. $BiVO_4$/GO/PANI photocatalyst with 3% mass ratio of PANI was produced by this method.

Characterization

The X-ray diffraction (XRD) decorations of the samples were precise by a D/MAX 2250 V diffractometer (Rigaku) using monochromatized Cu Kα ($\lambda = 0.15418$ nm) radiation beneath 40 kV and 100 mA and scanning above the range of ($10 \leq 2\theta \leq 70$ degrees). The morphologies and microstructures of the as-equipped samples were investigated by scanning electron microscope (SEM; JEOL JSM-6700F) and transmission electron microscope (TEM; JEOL JEM-2100F; accelerating voltage, 200 kV). Fourier transforms infrared (FTIR) spectra were recorded by a Bruker VECTOR 22 spectrometer by means of the KBr pellet technique. Raman spectra were acquired on a Renishaw inVia Reflex Raman Microprobe. UV–Vis diffuse reflectance spectra (DRS) of the as-organized samples were obtained by a Shimadzu UV-2550 spectrophotometer outfitted with an integrating sphere using $BaSO_4$ as the reflectance standard. X-ray photoelectron spectroscopy (XPS) analysis of the sample was passed out on a Physical Electronics PHI 1600 ESCA system operating at pass energy of 187.85 eV with an Al Kα X-ray source (E = 1486.6 eV). All binding energies of the composing elements were referenced to the C1*s* peak at 284.6 eV. UV–Vis diffuse reflectance spectra of the samples were conquered by an UV–Vis spectrophotometer (Hitachi U-3010), using H_2O as the reference.

Photocatalytic activity measurements

The photocatalytic activities of the samples were evaluated by the photocatalytic degradation of methylene blue (MB) and safranin O under visible light. A 500 W Xe lamp with a 420-nm cut-off filter was utilized as the light source to give visible-light irradiation. For the degradation of MB and SO, 0.1 g of photocatalyst was added to 100 mL of MB or safranin O solution (1×10^{-5} to 1×10^{-4} M). Dye solutions were made under visible light ($\lambda \geq 420$ nm) in a home-grown reactor with a cooling water circulator to maintain the reactor at a steady temperature. Before illumination, the solution was agitated for 120 min in the dark to achieve adsorption–desorption

equilibrium among the photocatalyst MB or safranin O dye. At 20-min intervals, a 7-mL solution was sampled. Then, the UV–visible absorption spectrum of the centrifuged solution was recorded by a Hitachi U-3010 UV–visible spectrophotometer.

Microbial safety test

Enterococcus aeruginosa, *Pseudomonas aeruginosa* and *E. coli* bacteria were screened for the safety test. *E. coli* K-12 strain of DH5a cells (Enzynomics) was pre-cultured and prepared as shown elsewhere, except for the number of bacterial cells used. Sixty-six *E. coli* cells were diluted with phosphate-buffered saline (PBS; Sigma-Aldrich) to 0.5×10 5 CFU/mL and dispensed (0.2 mL) on the film containing $BiVO_4$, $BiVO_4$/GO and $BiVO_4$/GO/PANI nanosheets. Bacterial cells dispensed on an empty well served as a control in the experiment. To avoid the vaporization of the bacterial cell solution on the surface, wet conditions were used during the microbial viability test. The bacterial cell suspension was harvested after 3-h incubation at 30 °C and the outward of the wafer washed thrice by pipetting with 1 ml of PBS. This was collected to harvest any remaining bacterial cells on the exterior. All the harvested bacterial cells were centrifuged and resuspended in 1 ml of PBS. Next, 150 µL of the suspension was spread on LB agar plates, and the colonies were counted after overnight incubation at 37 °C to estimate the loss of viability of *E. coli* cells on the $BiVO_4$, $BiVO_4$/GO and $BiVO_4$/GO/PANI nanosheet surfaces. All experiments were carried out in triplicate and repeated at least twice. Loss of viability was calculated using the following formula:

Loss of viability (%) = (counts of control − counts of samples incubated with 2D nanosheet surfaces)/counts of control × 100 (%).

Results and discussion

Characterizations of $BiVO_4$/GO/PANI sample

Figure 1 presents the XRD patterns of the prepared photocatalysts. Ten characteristic peaks of $BiVO_4$ can be found at $2\theta = 18.99°$, 28.95°, 30.55°, 34.49°, 35.22°, 42.46°, 46.71°,47.30°, 50.31° and 53.31° corresponding to the (110), (121), (040), (200), (002), (211), (060), (240), (222) and (161) crystal faces of the clinobisvanite structure (PDF 14-0688) [18, 19]. The characteristic peaks are matched with the value of clinobisvanite $BiVO_4$ reported in JCPDS 14-0688. The characteristic clinobisvanite $BiVO_4$ diffraction peaks occur clearly and simultaneously in the XRD pattern of $BiVO_4$/GO and $BiVO_4$/GO/PANI, which prove the successful synthesis of $BiVO_4$ in nanocomposites. In the XRD pattern of the $BiVO_4$/GO/PANI nanocomposites, all the peaks corresponding to $BiVO_4$ were also present, suggesting that the state of $BiVO_4$ did not change during the synthesis process. On the other hand, a slight reduction in the peak intensity was observed for $BiVO_4$ peaks in the $BiVO_4$/GO/PANI [20]. This might be due to the surface coating of PANI on GO and $BiVO_4$ during the synthesis process and the interactions between the GO, $BiVO_4$ nanoparticles

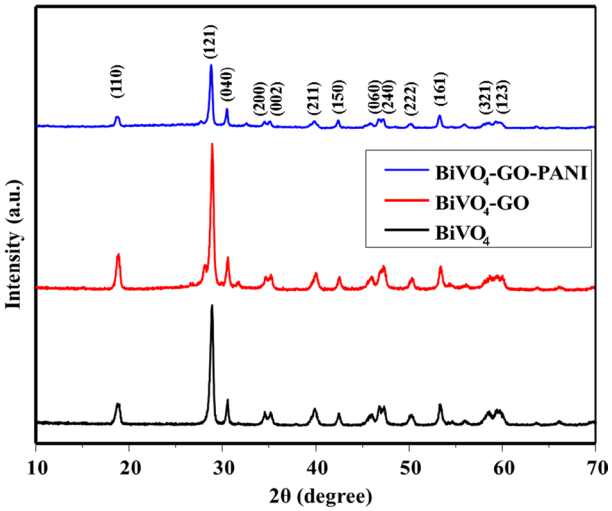

Fig. 1 XRD result of pure $BiVO_4$; $BiVO_4$/graphene oxide ($BiVO_4$–GO); $BiVO_4$/graphene oxide/polyaniline ($BiVO_4$–GO–PANI) with their index

and the PANI chain [21]. The presence of very sharp peaks in the XRD pattern of $BiVO_4$ indicates the well-defined crystalline structure. However, the diffraction peaks of GO and PANI are too weak to be found relative to the strong diffraction peaks of $BiVO_4$, perhaps because the diffraction peaks of GO become wider and less intense because of GO's lower crystallinity. In addition, the content of PANI is very low, so the XRD signal is not easily observed.

Furthermore, to that, no deflection peaks assigned to PANI were detected, which also recommended that the PANI layer was very thin [14].

Figure 2 shows typical SEM images of the as-prepared GO, $BiVO_4$/GO and $BiVO_4$/GO/PANI photocatalyst. The $BiVO_4$ has a significantly greater volume than PANI. Figure 2 shows that the product showed a layered structure with platelet-like morphology. A close-up view of the spherical (Fig. 2) shows that the majority of the crystals possess a non-uniform disordered shape with a center diameter of about 200 nm and length 400 nm. The GO particle intercalated homogenously with polymer; however, the $BiVO_4$ is staggered on the surface [12, 15]. In addition, such an amorphous structure was also shown by TEM investigation as displayed in Fig. 3. Closer inspection revealed that $BiVO_4$/GO/PANI contained many smaller nanoparticles with a size of about 100 nm. Figure 3 shows the polycrystalline rings resulting from the accumulation of the nanoparticles by a favored orientation. The surfaces of the graphene are coated by PANI nanoparticle. Small $BiVO_4$ particles are distributed on the surface of PANI. Figure 3d reveals that PANI is surrounded by a few $BiVO_4$ particles. Compared to Fig. 3b, the pure $BiVO_4$, the surface of the prepared $BiVO_4$/GO/PANI nanocomposites was not smooth anymore, but with a rough surface instead due to the coating of PANI nanoparticles, which could increase the reaction surface of the samples and provide more active sites, resulting in enhanced photocatalytic activity and performance [11, 12].

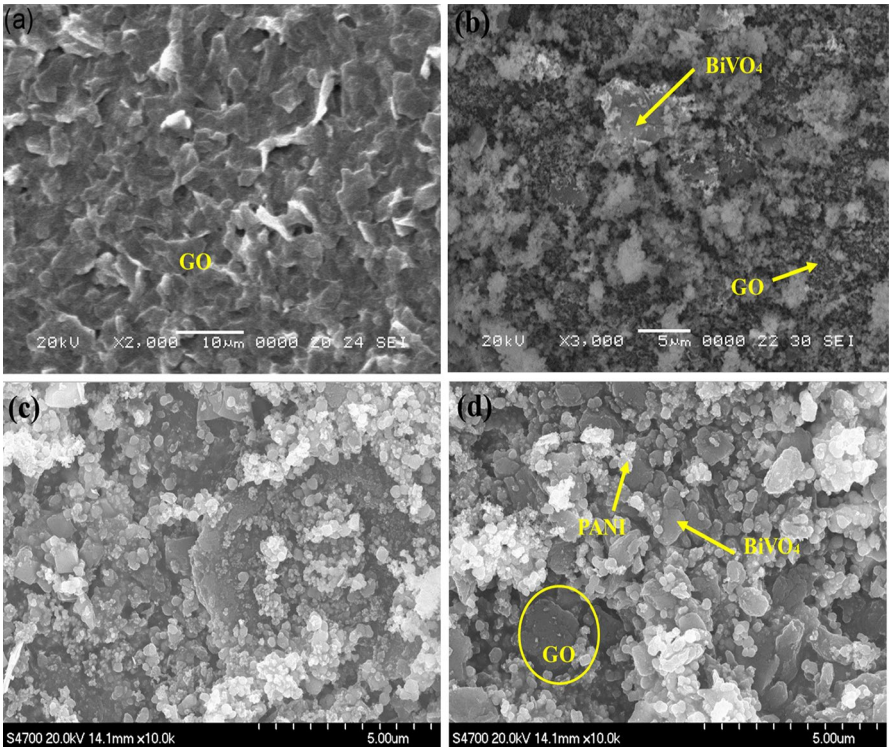

Fig. 2 SEM image of different kinds of samples, **a** GO, **b** $BiVO_4$/graphene oxide ($BiVO_4$–GO), **c** $BiVO_4$–GO–PANI, **d** $BiVO_4$/graphene oxide/polyaniline ($BiVO_4$–GO–PANI) (produced by hydrothermal process)

It has also been informed that smaller grain size and high crystallinity endowed higher photocatalytic action for the improved reactive sites and stimulated electron–hole departure efficiency [34, 35]. Thus, the as-prepared nano-$BiVO_4$/GO/PANI was estimated to show improved photocatalytic performance.

To confirm the effective transmission of GO and to characterize the carbon species, FTIR was used to get extra perception into the arrangement of GO, $BiVO_4$ and PANI. Figure 4 shows the FTIR spectra of $BiVO_4$, $BiVO_4$/GO and $BiVO_4$/GO/PANI, respectively. We estimated to detect a durable absorption band of GO at 3010 cm^{-1}, due to the O–H stretching vibration. However, after GO was joined with $BiVO_4$ and PANI, the peak strength reduced. The typical peaks at 1567 cm^{-1} can be credited to unoxidized carbon backbone [31, 32]. It was noted that the numerous oxygen-holding groups ((800–1900) cm^{-1}) in $BiVO_4$/GO and $BiVO_4$/GO/PANI significantly reduced or even extinct, showing that the hydrothermal synthesis is an effective technique for the synthesis of $BiVO_4$/GO/PANI. In the event of the $BiVO_4$/GO, the characteristic absorption peaks of GO are radically decreased or even vanished, as related to those of the unpolluted GO [36]. The extensive absorption cases at a short frequency (below 1000 cm^{-1}) are associated

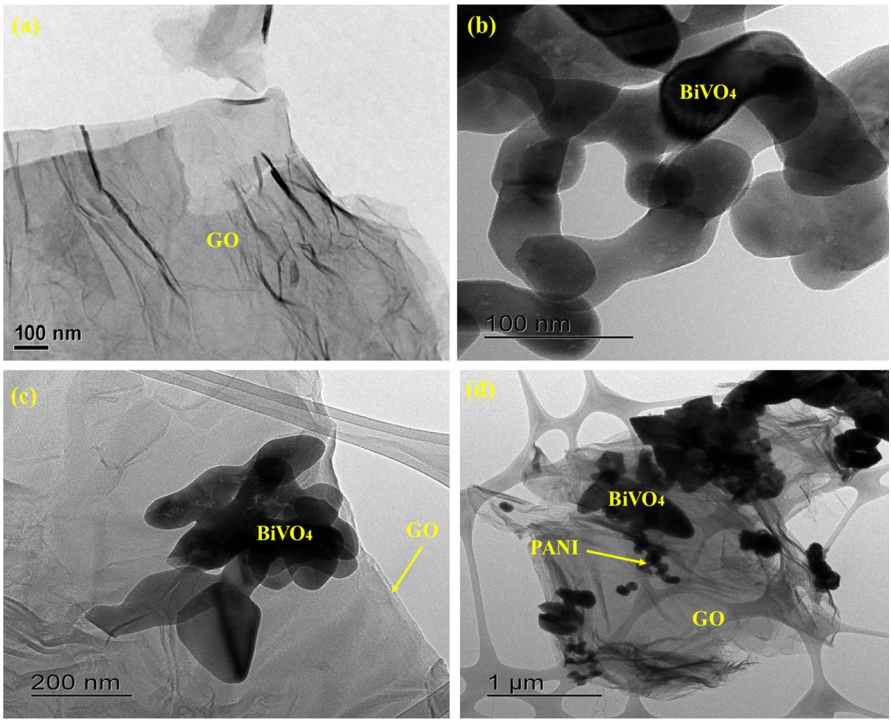

Fig. 3 TEM image of different kinds of samples, **a** GO, **b** $BiVO_4$, **c** $BiVO_4$/graphene oxide ($BiVO_4$–GO), **d** $BiVO_4$/graphene oxide/polyaniline ($BiVO_4$–GO–PANI) (produced by hydrothermal process)

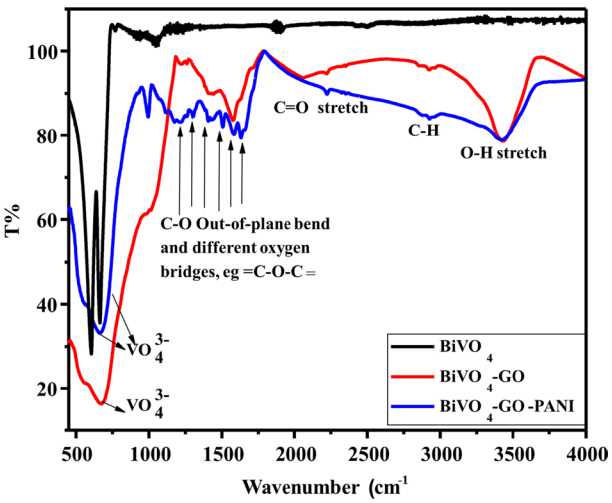

Fig. 4 FTIR result of different kinds of samples, **a** $BiVO_4$, **b** $BiVO_4$/graphene oxide ($BiVO_4$–GO), **c** $BiVO_4$/graphene oxide/polyaniline ($BiVO_4$–GO–PANI)

with (VO_4) and (VO_4). All the outcomes explain that in our study work, we can effectively organize a compound catalyst that incorporates GO as a platform.

Optical absorption of the as-prepared $BiVO_4$, $BiVO_4$/GO and $BiVO_4$/GO/PANI samples was measured by UV–visible DRS spectrometry. Figure 5 displays that the $BiVO_4$ sample has photoabsorption from UV light to visible light and the wavelength of the absorption edge is 525 nm [38]. The absorption of the PANI-modified $BiVO_4$/GO sample upturns over the complete range of the spectrum. On the basis of the equation $(ahv)^2 = A\ (hv - Eg)$ [39], the band gaps of the samples were estimated to be 2.42, 2.3 and 2.21 eV from the creation of the absorption edges, corresponding to the $BiVO_4$, $BiVO_4$/GO and $BiVO_4$/GO/PANI samples. This shows that the bandgap energy of the $BiVO_4$/GO/PANI sample is lesser than that of the $BiVO_4$. Therefore, the PANI-modified $BiVO_4$/GO sample can be able to energize generation of more electron–hole pairs under a similar visible-light illumination, which might result in upper photocatalytic action.

It is detected that $BiVO_4$ has a monoclinic phase, established on the attribute stretching vibrations and bending vibrations of the VO_4^{3-} tetrahedron (Fig. 6). The Raman spectrum of $BiVO_4$/GO/PANI shows two characteristic bands at 367 and 823 cm^{-1} which exhibit that $BiVO_4$ has a monoclinic phase, based on the attribute stretching vibrations and twisting vibrations of the VO_4^{3-} tetrahedron. The Raman spectrum of $BiVO_4$/GO/PANI illustrates two characteristic bands at 1355 and 1600 cm^{-1}, consistent to the *D* band and *G* band of GO, respectively [37]. Comparatively, in the $BiVO_4$, $BiVO_4$/GO and $BiVO_4$/GO/PANI composites, the *D* band and *G* band are slightly blue- and redshifted to 1346 and 1606 cm^{-1}, respectively, which may be produced by the altered surface strain, due to the interaction between GO and $BiVO_4$.

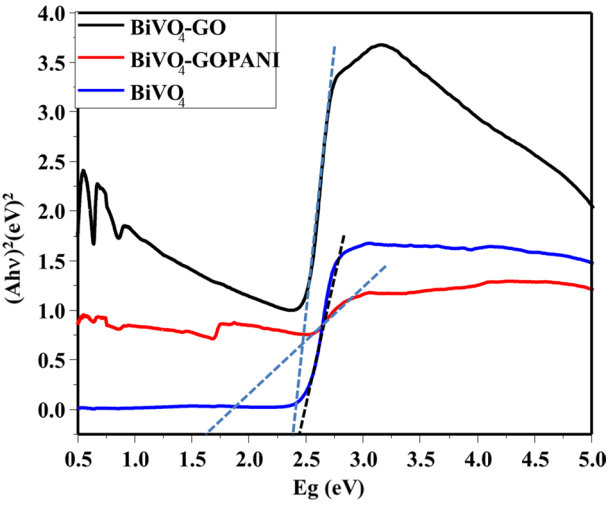

Fig. 5 DRS result of different kinds of samples, **a** $BiVO_4$, **b** $BiVO_4$/graphene oxide ($BiVO_4$–GO), **c** $BiVO_4$/graphene oxide/polyaniline ($BiVO_4$–GO–PANI)

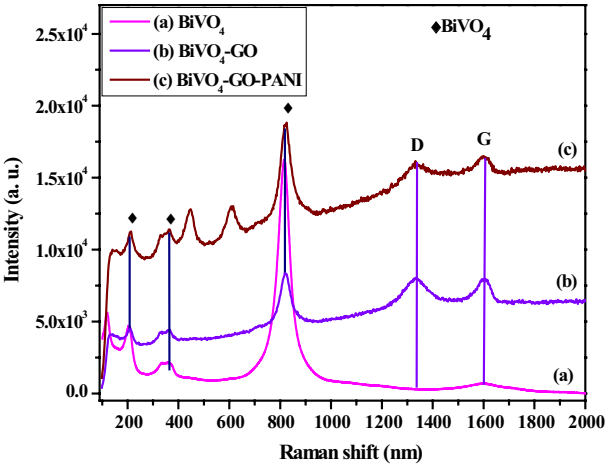

Fig. 6 Raman shift of different kinds of samples, **a** $BiVO_4$, **b** $BiVO_4$/graphene oxide ($BiVO_4$–GO), **c** $BiVO_4$/graphene oxide/polyaniline ($BiVO_4$–GO–PANI)

This occurrence is reliable with that detected in the hydrothermal in situ preparation of the $BiVO_4$/GO/PANI ($BiVO_4$, $BiVO_4$/GO and $BiVO_4$/GO/PANI) composites [32], where the D/G ratio (close to zero) proposes the effective combination of $BiVO_4$/GO with PANI polymer.

The configuration of the $BiVO_4$/GO/PANI heterogeneous nanostructures has been examined by X-ray photoelectron spectroscopy (XPS). Figure 7 shows high-resolution XPS spectra of the as-prepared $BiVO_4$/GO/PANI heterogeneous nanostructures. Figure 7a shows the binding energies located at about 160.1 and 166.5 eV that correspond to the $Bi4f_{5/2}$ and $Bi4f_{7/2}$ bands. Figure 7b displays the XPS spectrum of the O1*s* band, showing that dissimilar oxygen species exist on the surface of $BiVO_4$/GO/PANI heterogeneous nanostructures. The binding energies located at about 532.2 and 533.1 eV are attributed to the O1*s* band of lattice oxygen of GO crystallites [41] and the O1*s* band of lattice oxygen of $BiVO_4$ crystallites [42], respectively. Figure 7c displays the high-resolution XPS spectrum, in which the V2*p* bands shown in the peaks at about 527 and 518.5 eV correspond to $V2p_{1/2}$ and $V2p_{3/2}$ bands. The XPS spectrum of the C1*s* band in Fig. 7d clearly shows one peak formed at 287.3 eV, which relates to the C1*s* bands of GO and PANI crystallites. The C1*s* peak is complemented by two satellites on the high-binding-energy side denoted by peaks I and II which are set at about 287.3 and 287.5 eV, respectively. The foremost peak in the XPS spectrum of the N1*s* band is known to be characteristic of N^{2-} and the shake-up satellite peaks are patent and diagnostic of an open $3p^4$ shell of N^{2-} state [39], showing the existence of PANI on the surface. The fact that XRD does not display evidence of a PANI phase, while XPS displays the outward existence of N^{2-} ions suggests that $-NH_2$ is

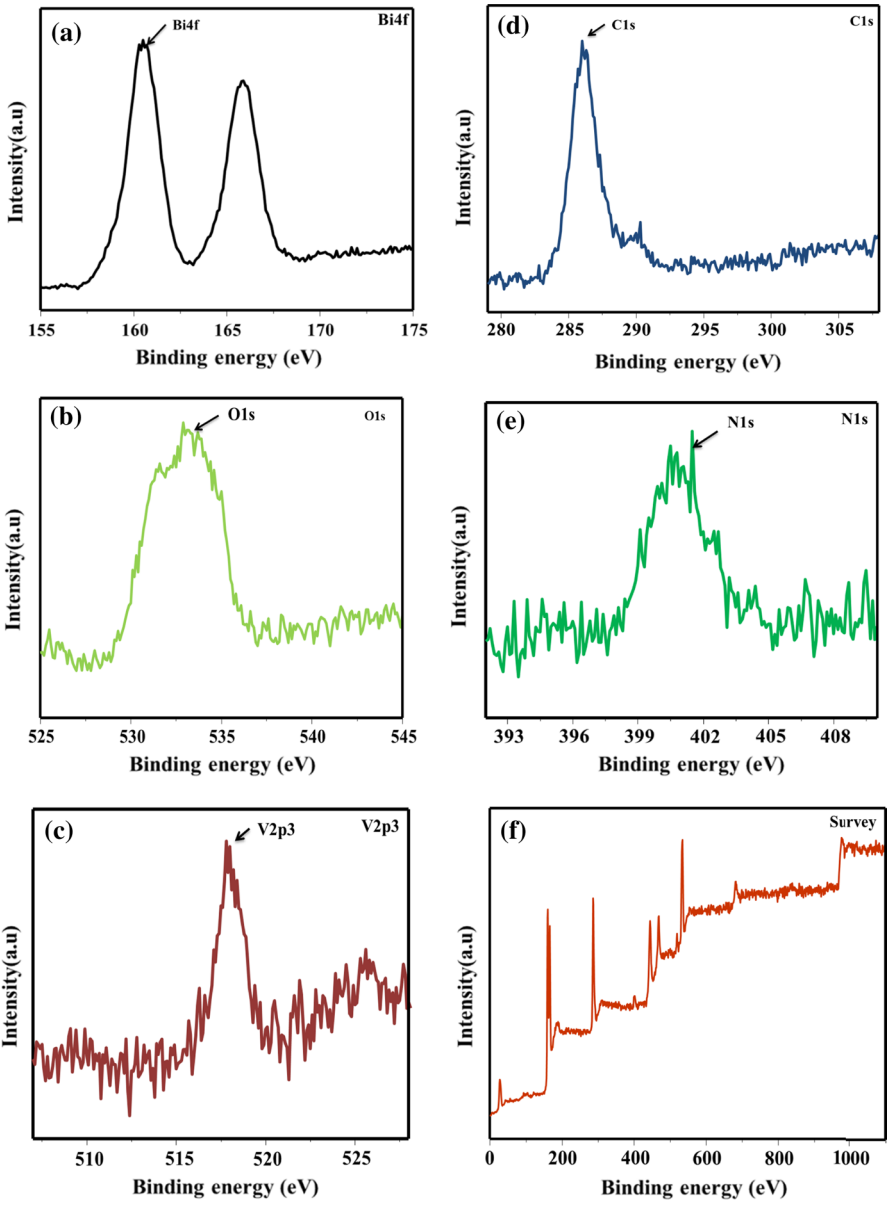

Fig. 7 XPS results of $BiVO_4$/graphene oxide/polyaniline ($BiVO_4$–GO–PANI) and $BiVO_4$–GO (samples **a**, **b**, **c**, **d**, **e**, **f**)

present only on the outward of the PANI nanocrystals and forms an exact skinny amorphous outer shell. According to the overhead experimental results of XRD, TEM and XPS, it can be realized that the N element is present in the system of NH^- on the exterior of the $BiVO_4$/GO/PANI heterogeneous nanostructures.

Visible-light-induced photocatalytic performance and mechanism on $BiVO_4$/GO/PANI

Photocatalytic degradation of dye

MB and safranin O were selected as representative hazardous dyes to define the photocatalytic performance of the as-equipped $BiVO_4$/GO/PANI which exhibited a major absorption band at 553 nm. Figures 8 and 9 display the respective photodegradation efficiencies of MB and safranin O that were mediated by photocatalysts under visible-light illumination ($\lambda > 420$ nm), with otherwise identical conditions. First, it was confirmed that the photolysis of MB and safranin O was slow for $BiVO_4$ photocatalyst under visible-light illumination. The adsorption of MB and safranin O on the $BiVO_4$/GO/PANI sample with dissimilar ratios in the dark was also checked. After 120 min, the concentrations of MB and safranin O decreased by 10% only. This suggests that the decolorizing of MB and safranin O by spherical-like $BiVO_4$/GO/PANI is mostly produced by photodegradation, but not adsorption. In addition to that, only 73% MB and 82% safranin O can be photodegraded by $BiVO_4$ under visible light in 180 min. However, all the $BiVO_4$/GO/PANI samples exhibited higher photocatalytic activities than $BiVO_4$. Among them, the $BiVO_4$/GO/PANI photocatalyst showed the maximum activity

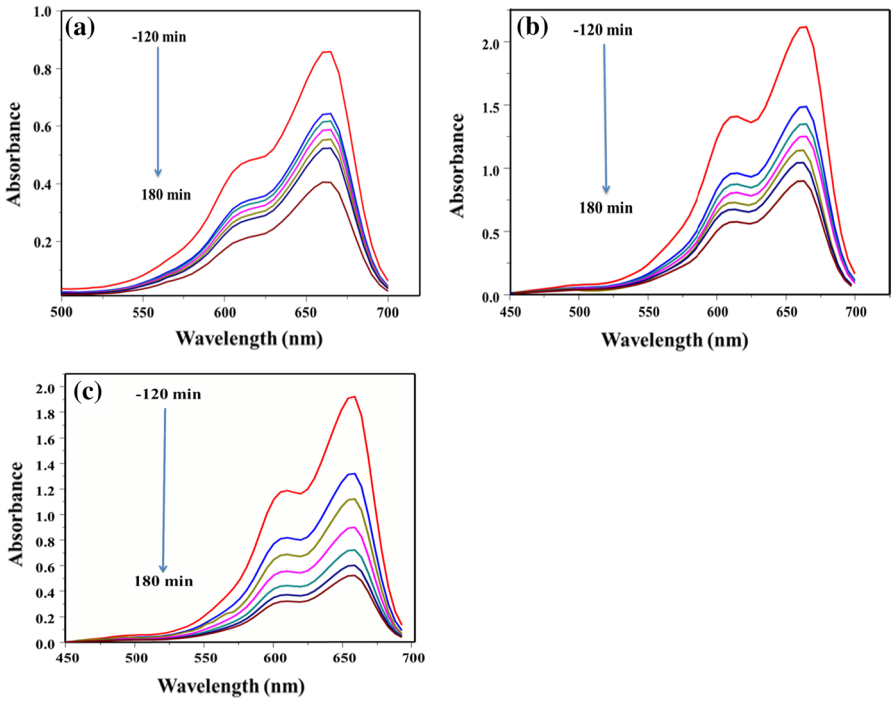

Fig. 8 Absorption changes of MB in the presence of **a** $BiVO_4$, **b** $BiVO_4$/graphene oxide ($BiVO_4$–GO), **c** $BiVO_4$/graphene oxide/polyaniline ($BiVO_4$–GO–PANI) samples

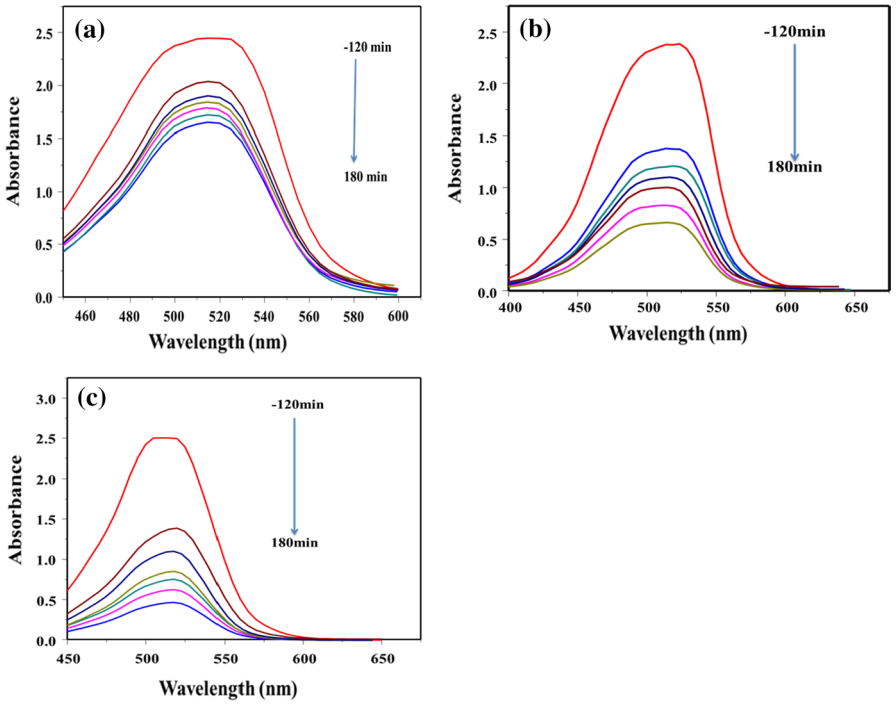

Fig. 9 Absorption changes of SO in the presence of **a** $BiVO_4$, **b** $BiVO_4$/graphene oxide ($BiVO_4$–GO), **c** $BiVO_4$/graphene oxide/polyaniline ($BiVO_4$–GO–PANI) sample

and photodegraded 73% MB and 82% safranin O after only 180 min under a similar condition. To quantitatively understand the response kinetics of the MB and safranin O degradation in our experiments, the Langmuir–Hinshelwood model was applied as expressed by Eq. (1), which is well known for the photocatalytic experiments when the pollutant is in the millimolar concentration range [42, 43].

$$-\ln\left(\frac{C}{C_0}\right) = kt \tag{1}$$

where C_0 and C are the concentrations of dye in solution at times 0 and t, respectively, and k is the apparent first-order rate constant. Figures 10 and 11 clearly show that in the plot of C/C_0 and time t, PANI had an excessive impact on the photodegraded rate (k) of the as-prepared samples. Table 1 show the list of the rate constant values. The sample with $BiVO_4$/GO/PANI showed the maximum photodegradation efficiency, which was about threefold, compared to that of the pure $BiVO_4$ sample. Figure 12 displays that the $BiVO_4$/GO/PANI has an excessive impact on the photodegradation rate (k) of the as-prepared samples.

Moreover, the improved photocatalytic activity after PANI and the photostability of the photocatalyst were also retained [15]. The circulating runs in the

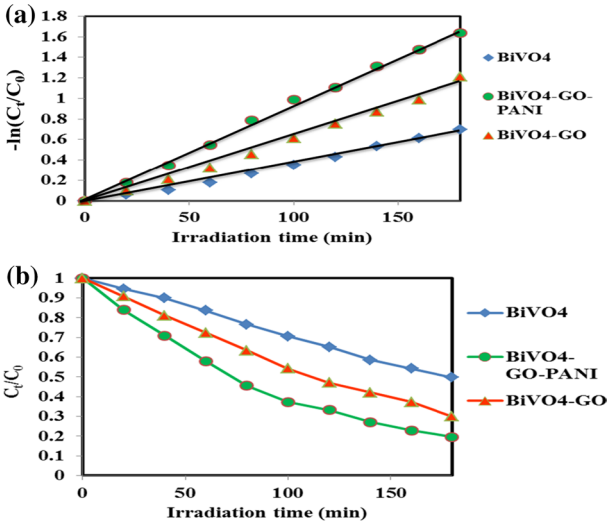

Fig. 10 **a** MB photodegradation as a function of illumination time for $BiVO_4$/graphene oxide/polyaniline ($BiVO_4$–GO–PANI), $BiVO_4$/graphene oxide ($BiVO_4$–GO) and $BiVO_4$ under visible light. **b** The plots of C_t/C_0 versus t for $BiVO_4$/graphene oxide/polyaniline ($BiVO_4$–GO–PANI), $BiVO_4$/graphene oxide ($BiVO_4$–GO) and $BiVO_4$. C_0 is the initial concentration of MB and C_t is the concentration at irradiation time t

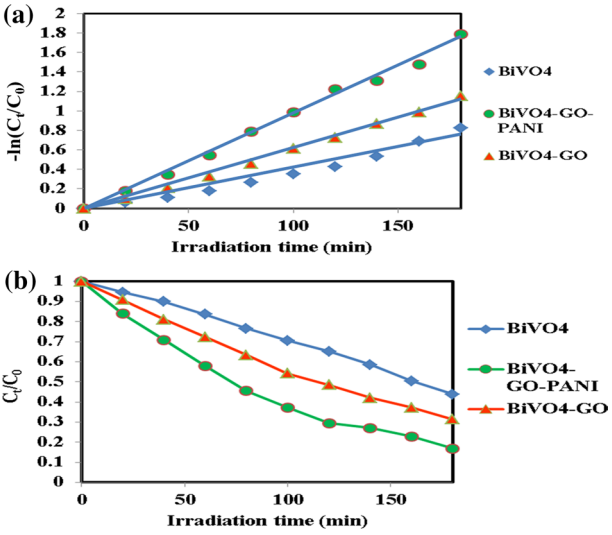

Fig. 11 **a** SO photodegradation as a function of illumination time for $BiVO_4$/graphene oxide/polyaniline ($BiVO_4$–GO–PANI), $BiVO_4$/graphene oxide ($BiVO_4$–GO) and $BiVO_4$ under visible light. **b** The plots of C_t/C_0 versus t for $BiVO_4$/graphene oxide/polyaniline ($BiVO_4$–GO–PANI), $BiVO_4$/graphene oxide ($BiVO_4$–GO) and $BiVO_4$. C_0 is the initial concentration of SO and C_t is the concentration at irradiation time t

Table 1 Apparent rate constant of MB and SO dyes

The apparent rate constant of different dyes				
Sample	MB		SO	
	$K^{-1}_{app(min)}$	R^2	$K^{-1}_{app(min)}$	R^2
$BiVO_4$	4.0×10^{-3}	0.9934	4.5×10^{-3}	0.9735
$BiVO_4$–GO	6.6×10^{-3}	0.9941	6.4×10^{-3}	0.9971
$BiVO_4$–GO–PANI	9.2×10^{-3}	0.9972	9.8×10^{-3}	0.995

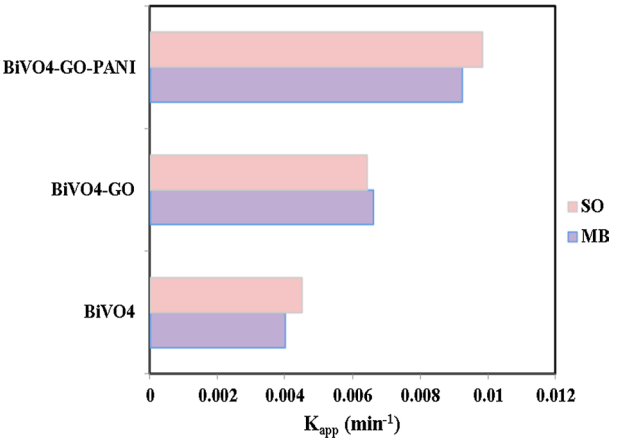

Fig. 12 Apparent rate constant of different kinds of samples versus different dyes by different catalysts

photocatalytic degradation of the attendance of $BiVO_4$/GO/PANI under visible light ($\lambda > 420$ nm) were checked after five reuses for the photodegradation of MB; the catalyst did not expose any vital loss of activity. This indicates that the $BiVO_4$/GO/PANI photocatalyst has high steadiness and does not photocorrode through the photocatalytic oxidation of the model pollutant molecules. PANI is cheaper than noble metals; so, the $BiVO_4$/GO/PANI photocatalyst is promising for practical application in water purification.

Photocatalytic mechanism

The above experiment demonstrates the tremendous photocatalytic performance of the as-prepared spherical-like $BiVO_4$/GO/PANI on the degradation of most commercial dyes. It follows that the PANI-modified $BiVO_4$/GO photocatalyst may have high potential applications in the conservation of the environment. Not only limited to the investigational results, but the photodegraded mechanism of dyes in the visible-light $BiVO_4$/GO/PANI structure was also vital to discover and guide the further improvement in its photocatalytic performance. The promising photocatalytic mechanism was estimated as follows:

$$BiVO_4 - GO - PANI \xrightarrow{h\vartheta} h^+ + e^- \quad (2)$$

Owing to the relative energy level of PANI (π-orbital and π*-orbital) and $BiVO_4$/GO (conduction band, CB, and valence band, VB) [13, 29], which leads to a synergetic effect, the photogenerated holes in VB can directly transport to the π-orbital of PANI. In this case, GO acts as an electron transferring media and helps electron–hole recombination (shown in Fig. 13).

Simultaneously, the photogenerated electrons can transport to the CB of $BiVO_4$, which results in charge separation and stabilization, hence hindering the recombination process. PANI is a high-quality substantial for transferring holes and the grain size of the photocatalyst is also comparatively minor [12]; so, the photogenerated charges can easily travel to the exterior of photocatalysts and photodegrade the adsorbed contaminations.

Investigation of safety aspects

There are various techniques for exploring the safety characteristics of nanomaterials such as colony counting method. This generally is used to verify the viability of bacteria by a live/dead fluorescent staining method by using impermeable propidium iodide dye where the viability of a cell is determined by the green or red color under confocal laser scanning microscope. Though, these are limited in tracing the bacterial cells that came in contact with the $BiVO_4$, $BiVO_4$/GO and $BiVO_4$/GO/PANI nanomaterials over time and observing the continuous change in the bacterial membrane for a detailed study on the antibacterial mechanism of $BiVO_4$, $BiVO_4$/GO and $BiVO_4$/GO/PANI nanomaterials.

To measure the special effects of the $BiVO_4$, $BiVO_4$/GO and $BiVO_4$/GO/PANI nanocomposite film, the volume and dry mass of individual bacteria were more calculated from the measured 3D RI tomograms. Figure 14 shows the relative dry mass and bacterial cell volume over time. The relative dry masses of live bacteria after 20 or 80 min of incubation on the $BiVO_4$, $BiVO_4$/GO and $BiVO_4$/GO/PANI

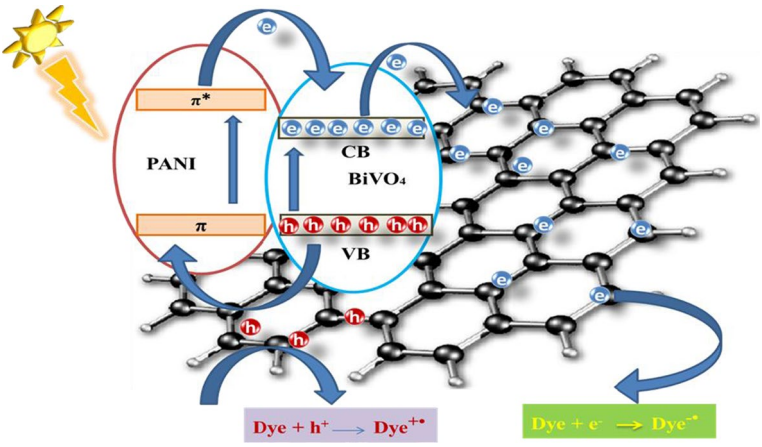

Fig. 13 Dye degradation mechanism with $BiVO_4$/graphene oxide/polyaniline nanocomposite

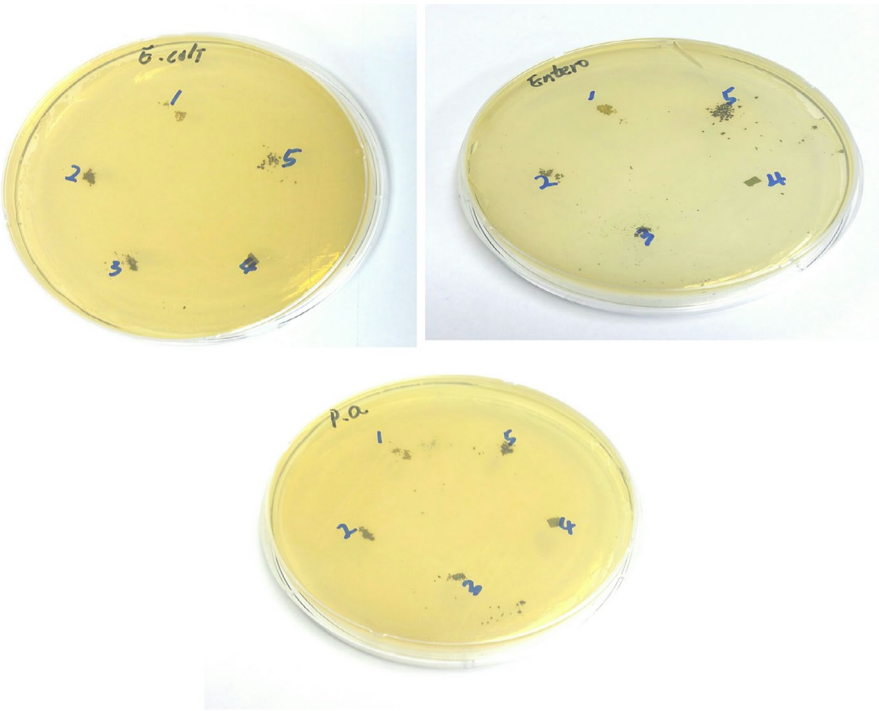

Fig. 14 Bactericidal test by **1** $BiVO_4$, **2** $BiVO_4$/graphene oxide ($BiVO_4$–GO), **3** $BiVO_4$–GO–PANI samples with three different kinds of bacteria **1** *E. Coli* = *Escherichia coli*, **2** Entero = *Enterococcus aeruginosa*, **3** P. A = *Pseudomonas aeruginosa*

nanocomposite film were intact. It was detected that the dry mass of live bacteria did not change substantially. These effects noticeably specify that $BiVO_4$, $BiVO_4$/GO and $BiVO_4$/GO/PANI nanocomposite film could not decrease both bacterial volume and dry mass, attended by damage of intracellular components and cell membranes.

Conclusions

For the first time, the spindle-like $BiVO_4$/GO/PANI photocatalyst was prepared by a hydrothermal process. The lesser grain size, an intrinsic belonging of PANI and the synergistic effect of PANI and $BiVO_4$/GO resulted in the rapid electron–hole separation and slow recombination. In consequence, the photodegradation of MB and safranin O with PANI-modified $BiVO_4$/GO photocatalysts under visible light ($\lambda > 420$ nm) was remarkably enhanced. The photocatalytic efficacy was also enhanced by the PANI. In addition to the enhanced photoactivity, the photostability of the photocatalyst was also retained. This work not only provides a mechanism for photocatalytic degradation but also opens a new perspective and gives some vision

into the design of newly improved photocatalysts with greater activity for environmental purification and other applications.

Compliance with ethical standards

Funding No funding was received in this study. It has been done by self-funding.

Conflict of interest The authors declare that they have no conflict of interest.

References

1. Xiao J, Xie Y, Cao H (2015) Organic pollutants removal in wastewater by heterogeneous photocatalytic ozonation. Chemosphere 121:1–17
2. Linsebigler AL, Lu G, Yates JT (1995) Photocatalysis on TiO_2 surfaces: principles, mechanisms, and selected results. Chem Rev 95:735–758
3. Li H, Yu H, Quan X, Chen S, Zhao H (2015) Improved photocatalytic performance of heterojunction by controlling the contact facet: high electron transfer capacity between TiO_2 and the 110 facet of $BiVO_4$ caused by suitable energy band alignment. Adv Func Mater 25:3074–3080
4. Ameen S, Seo HK, Akhtar MS, Shin HS (2012) Novel graphene/polyaniline nanocomposites and its photocatalytic activity toward the degradation of rose Bengal dye. Chem Eng J 210:220–228
5. Yuan H, Liu J, Li J, Li Y, Wang X, Zhang Y, Jiang J, Chen S, Zhao C, Qian D (2015) Designed synthesis of a novel $BiVO_4$–Cu_2O–TiO_2 as an efficient visible-light-responding photocatalyst. J Colloid Interface Sci 444:58
6. Liao G, Chen S, Quan X, Zhang Y, Zhao H (2011) Remarkable improvement of visible light photocatalysis with PANI modified core–shell mesoporous TiO_2 microspheres. Appl Catal B 102:126–131
7. Nanakkal AR, Alexander LK (2017) Graphene/$BiVO_4$/TiO_2 nanocomposite: tuning band gap energies for superior photocatalytic activity under visible light. J Mater Sci 52:7997–8006
8. Dreyer DR, Park S, Bielawski CW, Ruoff RS (2009) The chemistry of graphene oxide. Chem Soc Rev Chem Soc Rev 39:228–240
9. Zhu Y, Murali S, Cai W, Li X, Suk JW, Potts JR, Ruoff RS (2010) Graphene and graphene oxide: synthesis, properties, and applications. Adv Mater 22:3906–3924
10. Zhu Z, Han Q, Yu D, Sun J, Liu B (2017) A novel p-n heterojunction of $BiVO_4$/TiO_2/GO composite for enhanced visible-light-driven photocatalytic activity. Mater Lett 209:379–383
11. Ahmad I, Koziol K, Deveci S, Kim HK, Kumar R (2018) Advancing the use of high-performance graphene-based multimodal polymer nanocomposite at scale. Nanomaterials 8(11):947
12. Paulchamy B, Arthi G, Lignesh BD (2015) A simple approach to stepwise synthesis of graphene oxide nanomaterial. J Nanomed Nanotechnol 6(1):1
13. Wang X, Zhang J, Zhang K, Zou W, Chen S (2016) Facile fabrication of reduced graphene oxide/CuI/PANI nanocomposites with enhanced visible-light photocatalytic activity. RSC Adv 6:44851–44858
14. Zhao J, Biswas MRUD, Oh WC (2019) A novel $BiVO_4$–GO–TiO_2–PANI composite for upgraded photocatalytic performance under visible light and its non-toxicity. Environ Sci Pollut Res 26(12):11888–11904
15. Pandey M, Balachandran M, Joshi GM, Ghosh NN, Vendan AS (2019) Superior charge discharge ability of reduced graphene oxide/Li-ion embedded polymer composite films. J Mater Sci: Mater Electron 30(3):2136–2145
16. Ventura SP, de Barros RL, Sintra T, Soares CM, Lima AS, Coutinho JA (2012) Simple screening method to identify toxic/non-toxic ionic liquids: agar diffusion test adaptation. Ecotoxicol Environ Saf 83:55–62
17. Kirby W, Bauer AW, Sherris JC, Turck M (1966) Antibiotic susceptibility testing by a standardized single disc method. Am J Clin Pathol 45:493–496

18. Hokimura S, Moniz SA, Handoko A, Tang J (2014) Enhanced photoelectrochemical water splitting by nanostructured $BiVO_4$–TiO_2 composite electrodes. J Mater Chem A 2:3948–3953
19. Miao J, Xie A, Li S, Huang F, Cao J, Shen Y (2016) A novel reducing graphene/polyaniline/cuprous oxide composite hydrogel with unexpected photocatalytic activity for the degradation of Congo red. Appl Surf Sci 360:594–600
20. Al-Hussaini S, Eltabie RK, Rashad MEE (2016) One-pot modern fabrication and characterizati on of TiO 2 @terpoly (aniline, anthranilic acid and o-phenylenediamine) core–shell nanocomposites via polycondensation. Polymer 101:328–337
21. Patil PT, Anwane RS, Kondawar SB (2015) Development of electrospun polyaniline/ZnO composite nanofibers for LPG sensing. Procedia Mater Sci 10:195–204
22. Wu W, Liang S, Shen L, Ding Z, Zheng H, Su W, Wu L (2012) Preparation, characterization and enhanced visible light photocatalytic activities of polyaniline/Bi_3 NbO_7 nanocomposites. J Alloy Compd 520:213–219
23. Lin YC, Hsu FH, Wu TM (2013) Enhanced conductivity and thermal stability of conductive polyaniline/graphene composite synthesized by in situ chemical oxidation polymerization with sodium dodecyl sulfate. Synth Met 184:29–34
24. Zhang K, Zhang LL, Zhao XS, Wu J (2010) Graphene/polyaniline nanofiber composites as supercapacitor electrodes. Chem Mater 22:1392–1401
25. Li H, Sun Y, Cai B, Gan S, Han D, Niu L, Wu T (2015) Hierarchically Z-scheme photocatalyst of Ag@ AgCl decorated on $BiVO_4$ (040) with enhancing photoelectrochemical and photocatalytic performance. Appl Catal B 170:206–214
26. Huang CM, Pan GT, Peng PY, Yang CK (2010) In situ DRIFT study of photocatalytic degradation of gaseous isopropanol over $BiVO_4$ under indoor illumination. J Mol Catal A: Chem 327:38–44
27. Yousefzadeh S, Faraji M, Moshfegh AZ (2016) Constructing $BiVO_4$/Graphene/TiO_2 nanocomposite photoanode for photoelectrochemical conversion applications. J Electroanal Chem 763:1–9
28. Jing L, Yang ZY, Zhao YF, Zhang YX, Guo X, Yan YM, Sun KN (2013) Ternary polyaniline-graphene-TiO_2 hybrid with enhanced activity for visible-light photo-electrocatalytic water oxidation. J Mater Chem A 2:1068–1075
29. Domingues SH, Salvatierra RV, Oliveira MM, Zarbin AJ (2011) Transparent and conductive thin films of graphene/polyaniline nanocomposites prepared through interfacial polymerization. Chem Commun 47:2592–2594
30. Li X, Teng W, Zhao Q, Wang L (2011) Efficient visible light-induced photoelectrocatalytic degradation of rhodamine B by polyaniline-sensitized TiO_2 nanotube arrays. J Nanopart Res 13:6813–6820
31. Biswas MRUD, Oh WC (2018) Synthesis of $BiVO_4$–GO–PVDF nanocomposite: an excellent, newly designed material for high photocatalytic activity towards organic dye degradation by tuning band gap energies. Solid State Sci 80:22–30
32. Yu J, Xiong J, Cheng B, Liu S (2005) Fabrication and characterization of Ag–TiO_2 multiphase nanocomposite thin films with enhanced photocatalytic activity. Appl Catal B 60(3–4):211–221
33. Geim AK, Novoselov KS (2007) The rise of graphene. Nat Mater 6(3):183
34. Azam A, Ahmed AS, Oves M, Khan MS, Habib SS, Memic A (2012) Antimicrobial activity of metal oxide nanoparticles against Gram-positive and Gram-negative bacteria: a comparative study. Int J Nanomed 7:6003
35. Reddy KR, Karthik KV, Prasad SBB, Soni SK, Han MJ, Raghu AV (2016) Enhanced photocatalytic activity of nanostructured titanium dioxide/polyaniline hybrid photocatalysts. Polyhedron 120:169–174
36. Biswas MRUD, Oh WC (2019) Comparative study on gas sensing by a Schottky diode electrode prepared with graphene–semiconductor–polymer nanocomposites. RSC Adv 9(20):11484–11492
37. Kim F, Cote LJ, Huang J (2010) Graphene oxide: surface activity and two-dimensional assembly. Adv Mater 22(17):1954–1958
38. Cote LJ, Kim J, Tung VC, Luo J, Kim F, Huang J (2010) Graphene oxide as surfactant sheets. Pure Appl Chem 83(1):95–110
39. Wang Y, Li Z, Wang J, Li J, Lin Y (2011) Graphene and graphene oxide: biofunctionalization and applications in biotechnology. Trends Biotechnol 29(5):205–212
40. Biswas MRUD, Cho KY, Jung CH, Oh WC (2019) Novel synthesis of $LaNiSbWO_4$–G–PANI designed as quaternary type composite for high photocatalytic performance of anionic dye and trihydroxybenzoic acid under visible-light. Process Saf Environ Prot 126:348–355

41. Xu Y, Mo Y, Tian J, Wang P, Yu H, Yu J (2016) The synergistic effect of graphitic N and pyrrolic N for the enhanced photocatalytic performance of nitrogen-doped graphene/TiO2 nanocomposites. Appl Catal B 181:810–817
42. Su W, Lu X, Jia S, Wang J, Ma H, Xing Y (2015) Catalytic reduction of NO_X Over TiO_2–graphene oxide supported with MnO_X at low temperature. Catal Lett 145(7):1446–1456
43. Dowla BMRU, Cho JY, Jang WK, Oh WC (2017) Synthesis of $BiVO_4$–GO–PTFE nanocomposite photocatalysts for high efficient visible-light-induced photocatalytic performance for dyes. J Mater Sci: Mater Electron 28(20):15106–15117

Publisher's Note Springer Nature remains neutral with regard to jurisdictional claims in published maps and institutional affiliations.